Inorganic Chemistry
Article
Cite This: Inorg. Chem. XXXX, XXX, XXX−XXX
pubs.acs.org/IC

A Key Factor Dominating the Competition between Photolysis and Photoracemization of $[Ru(bipy)_3]^{2+}$ and $[Ru(phen)_3]^{2+}$ Complexes

Lixia Feng[†,‡] and Yuekui Wang*[,†]

[†]Key Laboratory of Chemical Biology and Molecular Engineering of the Education Ministry, Institute of Molecular Science, Shanxi University, Taiyuan, Shanxi 030006, P. R. China

[‡]Department of Chemistry, Taiyuan Normal University, Jinzhong, Shanxi 030619, P. R. China

Supporting Information

ABSTRACT: Photolysis and photoracemization are two important photochemical phenomena of the prototype complexes $[Ru(bipy)_3]^{2+}$ and $[Ru(phen)_3]^{2+}$ (bipy = 2,2′-bipyridine, phen = 1,10-phenanthroline), but little is known about their relations. To solve this issue, the photoinduced chiral inversion $\Delta \rightleftharpoons \Lambda$ of the complexes was analyzed theoretically. The results indicated that the photoracemization reaction proceeds on the lowest triplet potential energy surface in three steps $^3CT_\Delta \leftrightarrow {}^3MC_\Delta$, $^3MC_\Delta \leftrightarrow {}^3MC_\Lambda$, and $^3MC_\Lambda \leftrightarrow {}^3CT_\Lambda$ (CT = charge transfer state; MC = metal-centered state). Where the first and third steps are fast processes of picoseconds, the second is the rate-determining step (RDS) of microseconds. Such a slow step for the racemization leads to the excited molecule lingering around the bottom of ^{3}MC state after the first step and, therefore, greatly enhances the possibility of deexcitation and photolysis mostly at the triplet-singlet crossing point. In other words, the photoracemization and photolysis of the complexes have a competition relation, not a slave relation as assumed by the photoracemization model suggested in literature. They are dominated by the RDS. This conclusion is also consistent with the $\Delta(\delta S) \rightleftharpoons \Lambda(\delta S)$ chiral inversion of the $[Ru(bipy)_2(L\text{-ser})]^+$ series complexes, which is reversible with no detectable photolysis, as its second step is a fast one. Note that, although the photoracemization of the prototype complexes is very slow, it passes through the three steps reversibly and ends with a photon emitting, which could be detected with the time-resolved circularly polarized luminescence and related techniques. These findings are helpful to understand and control the photochemical behavior of the complexes in practice.

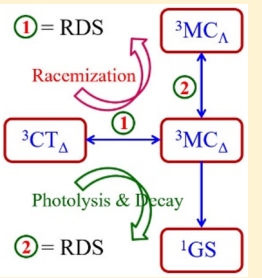

INTRODUCTION

As prototype compounds of photochemistry and photophysics,[1−3] the ruthenium tris-diimine complexes $[Ru(bipy)_3]^{2+}$ and $[Ru(phen)_3]^{2+}$ (bipy = 2,2′-bipyridine, phen = 1,10-phenanthroline) have been studied extensively for one-half century[4,5] due to their extraordinary importance in the photochemistry and photophysics and extensive application in many fields.[6−11] Now it is clear that these chelates exhibit various photochemical activities when exposed to light, such as photolysis,[12,13] photosubstitution,[14,15] photoracemization,[16] etc., though they are chemically very stable in the ground state.[17,18] A detailed mechanism for both the photosubstitution and photoracemization of $[Ru(bipy)_3]^{2+}$ has been proposed.[12] However, the mechanism suggested for the photoracemization of $[Ru(bipy)_3]^{2+}$ might be debatable, because it involves a rearrangement of the square pyramidal primary photoproduct into a trigonal bipyramidal intermediate, which is not self-consistent with other observations for related systems. For example, later experiment[19] on the formation of ruthenium tris-diimine complexes with a chiral derivative of 2,2′-bipyridine gave no evidence for such inversion process. It cannot yet be used to account for the $\Delta(\delta S) \leftrightarrow \Lambda(\delta S)$ photoinduced chiral inversion at the Ru(II) center of *cis*-$[Ru(bipy)_2(aa)]^+$ (aa is an optically active amino acid anion) complexes,[20,21] because this is a unique class of photoinduced reversible chiral inversion with neither ligand release nor substitution in the coordination sphere. Previously, we have reported[22] a theoretical analysis on the photoinduced chiral inversion of $[Ru(bipy)_2(L\text{-ser})]^+$ (L-ser = L-serine) and found that the chiral inversion proceeds actually on a metal centered triplet ground-state ^{3}MC due to the crossover of the triplet T_1 and singlet S_0 states. Examining the transient geometries at the crossing points, we found that their imaginary or lowest-frequency displacement vector in the T_1 state still dominates the inversion path, which makes the key transition state ^{3}TS avoid the fate of ligand dissociations and fast decay and, therefore, insures the chiral inversion to be reversible. We thought that such a triplet ground-state bridged photochemical mechanism is also a starting point to understand the photochemical phenomena of the prototype ruthenium tris-diimine complexes, not only for the photoracemization but also for the photolysis and photosubstitutions.

In the current Paper, a theoretical analysis on the photoracemization of the prototype complexes $[Ru(bipy)_3]^{2+}$ and $[Ru(phen)_3]^{2+}$ is reported. The main object is to clarify the photochemical reaction pathways in a self-consistent way. Particular attention is paid to elucidating the mechanism that dominates the competition between photoracemization and photolysis of the complexes. Such knowledge may offer a

Received: April 11, 2018

DOI: 10.1021/acs.inorgchem.8b00975
Inorg. Chem. XXXX, XXX, XXX−XXX

comprehensive understanding on the photochemical and photophysical properties of the complexes.

CALCULATION SCHEME AND COMPUTATIONAL DETAILS

Calculation Scheme. The photoinduced racemization of $[Ru(bipy)_3]^{2+}$ and $[Ru(phen)_3]^{2+}$ involves both photophysical and photochemical processes. The initial Δ (or Λ) isomer is excited into one of the singlet excited states by irradiation first, then relaxes to the lowest triplet state T_1 via rapid nonradiative intersystem crossing (ISC). This is a ultrafast photophysical process.[23] From the triplet state T_1 of the reactant (Δ-isomer) to the corresponding state T_1 of the product (Λ-isomer) is the photochemical process, which usually consists of three steps with three transition states, as schematically illustrated in Figure 1. Where $^3CT_\Delta$ and $^3MC_\Delta$ are, respectively, the

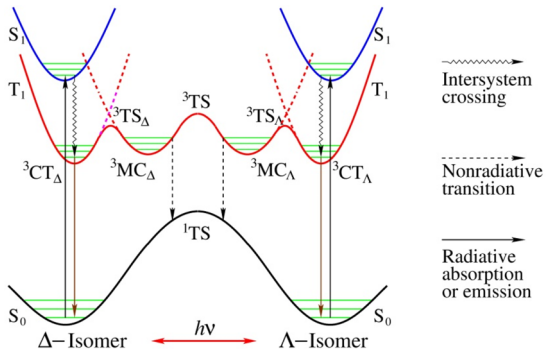

Figure 1. Schematic illustration of the excited states and related transition states in the photoracemization of the ruthenium tris-diimine complexes along the relaxed S_0 pathway.

lowest-energy metal-to-ligand charge transfer (MLCT) and metal-centered or ligand field[24,25] (MC) excited states of the Δ-isomer, $^3TS_\Delta$ is the related transition state. Similarly, $^3CT_\Lambda$, $^3MC_\Lambda$, and $^3TS_\Lambda$ are the corresponding states of the Λ-isomer. From $^3MC_\Delta$ to $^3MC_\Lambda$ is the most important step for the racemization; the corresponding transition state is ^3TS. In this step, some nonradiative transition or decay may occur, as indicated by the dashed vertical lines.

To determine the energies and geometries of these excited states reasonably, it is necessary to discuss the ground-state (S_0) geometries of the Δ/Λ-isomers as well as the possible structures of the transition state ^1TS first, because they provide a good initial guess for the corresponding excited states $^3CT_\Delta$, $^3CT_\Lambda$, and ^3TS. The related metal-centered states $^3MC_{\Delta/\Lambda}$ could be found along the imaginary frequency displacement vector of the ^3TS. Finally, search the two transition states $^3TS_\Delta$ and $^3TS_\Lambda$ using geometry interpolation method. We believe that this calculation scheme could be the most natural one if not unique, because the chiral inversion on the ground state for a six-coordinated metal complex are known, that is, the one-step Bailar[26] and Ray-Dutt[27] twists, as well as the bond-rupture models,[28] though the latter may not be adequate for our purpose due to their multistep characteristics.

Computational Details. Since the Δ and Λ isomers of the title complexes are a pair of enantiomers, only one of them need be calculated. The geometry optimizations for reaction on the ground (S_0) and triplet excited (T_1) states were performed using the density functional theory (DFT) method with the B3LYP[29] hybrid functional. The core orbitals of ruthenium are represented by the quasi-relativistic Stuttgart ECP28MWB pseudopotential,[30] and a fairly larger basis set[31] with the splitting pattern (8s7p6d2f)/[6s5p3d2f]-{311111/22111/411/11} is used for its valence electrons, while the polarized triple-ζ 6-311G(d) basis set is used for other atoms. Frequency calculations were performed for all the optimized structures involved in the reaction to confirm the stationary points as local minima or transition states (with one imaginary frequency). The transition states ^1TS in both Bailar and Ray-Dutt twists on the ground state (S_0) were verified by the intrinsic reaction coordinate (IRC)[32] calculation, and those ^3TS, $^3TS_\Delta$/$^3TS_\Lambda$ for the triplet state (T_1) were fully confirmed by geometry optimization along the imaginary-frequency displacement vector of the normal mode. The triplet states ^3CT, ^3MC, and ^3TS, etc., were characterized by spin-density analysis.[33] The energies of the related vertical states were obtained using the time-dependent density functional theory (TDDFT) method with the same functional and basis set. All calculations were performed using the Gaussian 09 program suite[34] with ultrafine integral grid and tight convergence criterion, and the solvent effect (aqueous solution) is considered with the polarizable continuum model (PCM).[35]

RESULTS AND DISCUSSION

Geometries of the Transition States ^1TS. To facilitate later discussion on the chiral inversion pathway, the optimized geometries of $[Ru(bipy)_3]^{2+}$ and $[Ru(phen)_3]^{2+}$ complexes, together with the labels of ligands and coordination atoms, are depicted in Figure 2. The corresponding Cartesian coordinates and selected bond parameters are collected in Table S1 (see the Supporting Information) and Table 1, respectively.

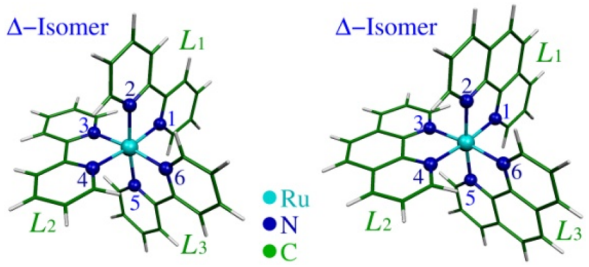

Figure 2. Labels of the coordination atoms and ligands for the $[Ru(bipy)_3]^{2+}$ (left) and $[Ru(phen)_3]^{2+}$ (right) chelates.

As mentioned in Calculation Scheme, there are two one-step mechanisms for the racemization of the complexes in the ground state, known as the Bailar[26] and Ray-Dutt[27] twists, respectively. The Bailar twist is performed by rotating the upper three coordinate atoms N_2, N_4, and N_6 of the ligands around the C_3-axis through a triangular prism (TS_B) to the opposite enantiomer, as depicted in Figure 3b. Similarly, the Ray-Dutt twist is performed by rotating the three coordinate atoms N_1, N_2, and N_3 about another C_3- or pseudo C_3-axis that only exists in the parent octahedral core $\{RuN_6\}$, as illustrated in Figure 3a. The latter owns a rhombic transition state TS_A with C_2- or pseudo C_2-symmetry. Therefore, they are usually called as *trigonal twist* and *rhombic twist*, respectively.

The geometries of ^1TS in both Bailar and Ray-Dutt twists were determined and summarized in Table S1. The selected bond parameters of the transient structures ^1TS_A and ^1TS_B, together with those of the Δ-enantiomer, are compiled in Table 1. It should be pointed out that all the geometry optimizations and transition-state searches were performed without symmetry constraints to avoid some artifactitious symmetry, but the results still exhibit certain symmetry approximately; for example, the Δ-enantiomer of S_0 and the structure of ^1TS_A are of D_3- and C_s-symmetric, respectively. One might anticipate the symmetry of ^1TS_B to be D_{3h}, but it is only C_3- (bipy)/C_s-symmetric (phen) or roughly C_{3h}-symmetric due to the spatial repulsion between ligands, which bends the ligands significantly (see Figure S1).

The total energies of ^1TS_A and ^1TS_B relative to the Δ-isomer are 2.596 and 3.562 eV for $[Ru(bipy)_3]^{2+}$ and 2.662 and 3.483

DOI: 10.1021/acs.inorgchem.8b00975
Inorg. Chem. XXXX, XXX, XXX−XXX

Table 1. Selected Bond Lengths (Å), Bond and Dihedral Angles (in deg) for the Reactant Δ Isomer and Transition States ^1TS_A and ^1TS_B

	$[Ru(bipy)_3]^{2+}$ (S_0)			$[Ru(phen)_3]^{2+}$ (S_0)		
chelate structure	Δ-isomer	^1TS_A	^1TS_B	Δ-isomer	^1TS_A	^1TS_B
$Ru-N_1$	2.088	2.086	2.156	2.094	2.080	2.177
$Ru-N_2$	2.088	2.087	2.186	2.094	2.080	2.177
$Ru-N_3$	2.088	2.036	2.155	2.095	2.035	2.177
$Ru-N_4$	2.088	2.128	2.185	2.094	2.172	2.177
$Ru-N_5$	2.088	2.285	2.154	2.094	2.355	2.179
$Ru-N_6$	2.088	2.288	2.183	2.095	2.355	2.179
mean	2.088	2.152	2.170	2.094	2.179	2.178
N_1-Ru-N_2	78.16	74.74	74.05	79.15	76.48	75.14
N_3-Ru-N_4	78.18	78.01	74.11	79.16	78.49	75.13
N_5-Ru-N_6	78.18	69.46	74.13	79.16	69.12	75.15
N_1-Ru-N_3	96.91	88.53	87.69	96.08	88.29	86.76
N_1-Ru-N_5	96.88	82.30	87.85	96.03	82.48	86.78
N_4-Ru-N_5	88.44	85.81	132.82	89.13	84.88	133.09
mean	86.12	79.81	88.44	86.45	79.96	88.68
$D(L_1L_2)$[a]	86.69	−90.18	119.50	87.84	−89.98	−120.25
$D(L_1L_3)$	86.69	70.58	120.24	87.84	−78.43	−120.30
$D(L_2L_3)$	86.50	89.42	120.17	88.00	90.01	−119.45

[a] $D(L_1L_2)$ is the dihedral angle between the ligands L_1 and L_2 (cf. Figure 2), which is determined by their planes of inertia.

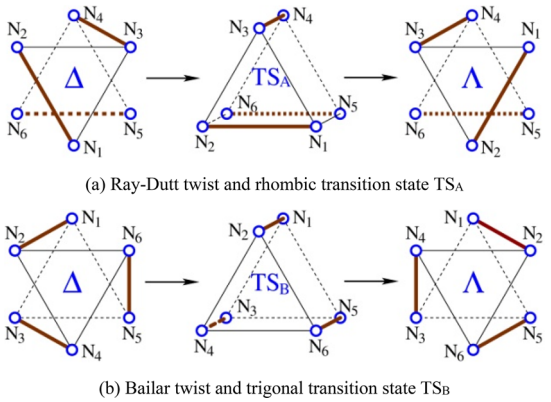

(a) Ray-Dutt twist and rhombic transition state TS_A

(b) Bailar twist and trigonal transition state TS_B

Figure 3. Schematic representation of the Ray-Dutt (a) and Bailar (b) twists for the racemization of $[Ru(bipy)_3]^{2+}$ and $[Ru(phen)_3]^{2+}$ complexes. The C_3- or pseudo C_3-axis is perpendicular to the page and passes through the central atom, as indicated by the Δ/Λ symbols.

eV for $[Ru(phen)_3]^{2+}$. Clearly, the Ray-Dutt rhombic twist is preferred than the Bailar trigonal prismatic one, though both barriers are too high to thermal activation, as expected. In addition, our calculations also showed that the averaged dissociation energy of Ru−N bonds for these chelates is ∼1.60 eV (∼37 kcal/mol). Therefore, the bond rupture model[28] for racemization of the complexes in the ground state is impossible. It might be applied to the photodissociation product that will be discussed in detail later.

Energies of the ^3TS and Related States. Take the structures of ^1TS_A and ^1TS_B as the initial geometries of the key transition state ^3TS and optimize them, and the results are confirmed to be the triplet transition states ^3TS_A and ^3TS_B. Then, optimize structures near the ^3TS_A or ^3TS_B at ca. ±10% of the imaginary frequency displacement vector, yielding two new geometries, which were characterized as the $^3MC_\Delta$ and $^3MC_\Lambda$ states by means of the NBO spin-density analysis,[33] as shown in Table 2 for the Δ enantiomers in rhombic twists. The $^3CT_\Delta$ state was located by reoptimizing the S_0 structures of the Δ isomer with the restriction of triplet state. Finally, the $^3TS_\Delta/^3TS_\Lambda$ transition state was obtained by optimizing the interpolation geometry between ^3CT and ^3MC states. Note that, since the energy of ^3TS_B is 13.5 kcal/mol higher than that of ^3TS_A for both complexes, the trigonal prismatic inversion is impossible and will not be discussed. Only the results for the rhombic inversion are listed in Tables S2 and S3. To facilitate discussion, the relative energies and Gibbs free energies at 298.15 K are compiled in Table 3. The corresponding structures are depicted in Figure 4, and the main bond parameters are tabulated in Table 4.

From Table 3 it is clear that the energy of ^3MC state for $[Ru(phen)_3]^{2+}$ is lower than that of ^3CT, while for $[Ru(bipy)_3]^{2+}$ the former is significantly higher than the latter. This indicates that they may have different photostability

Table 2. Spin-Density Distribution of the ^3CT, ^3MC, and ^3TS Triplet States for $[Ru(bipy)_3]^{2+}$ and $[Ru(phen)_3]^{2+}$ in the Rhombic Twist[a]

	$[Ru(bipy)_3]^{2+}$ (T_1)				$[Ru(phen)_3]^{2+}$ (T_1)			
triplet states	$^3CT_\Delta$	$^3TS_\Delta$	$^3MC_\Delta$	$^3TS_\Lambda$	$^3CT_\Delta$	$^3TS_\Delta$	$^3MC_\Delta$	$^3TS_\Lambda$
Ru	0.9229	1.3521	1.7633	1.7422	0.9218	1.2830	1.7934	1.7595
L_1	0.0113	0.1661	0.1105	0.1075	0.0108	0.1098	0.0961	0.1001
L_2	1.0543	0.4676	0.1145	0.0428	1.0547	0.4763	0.0961	0.0402
L_3	0.0114	0.0141	0.0117	0.1075	0.0127	0.1309	0.0144	0.1001

[a] The spin-density of a ligand is the sum of atom spin-densities involved in the ligand.

DOI: 10.1021/acs.inorgchem.8b00975
Inorg. Chem. XXXX, XXX, XXX−XXX

Table 3. Relative Energies[a] of the ^{3}CT, ^{3}MC, and ^{3}TS Triplet States in the Photoinduced Racemization of $[Ru(bipy)_3]^{2+}$ and $[Ru(phen)_3]^{2+}$

	$[Ru(bipy)_3]^{2+}$ (T_1)				$[Ru(phen)_3]^{2+}$ (T_1)			
triplet states	E_{el}	E_0	$G^{\ddagger}$	ν_0	E_{el}	E_0	$G^{\ddagger}$	ν_0
$^3CT_\Delta$	0.000	0.000	0.000	29.7	0.000	0.000	0.000	20.1
$^3TS_\Delta$	4.658	3.589	2.679	*i*231.7	3.831	3.303	2.818	*i*216.9
$^3MC_\Delta$	1.928	2.095	0.342	20.4	−0.956	−0.493	−2.506	20.2
$^3TS_\Lambda$	9.262	9.650	9.121	*i*37.7	7.013	7.930	7.920	*i*29.5

[a] E_{el}, E_0, and $G^{\ddagger}$ are the electron energy, total energy with the zero-point energy (ZPE) correction, and relative Gibbs free energy at 298.15 K, respectively (in kcal/mol). ν_0 is the lowest vibrational frequency (in cm^{-1}) or imaginary frequency for the transition state.

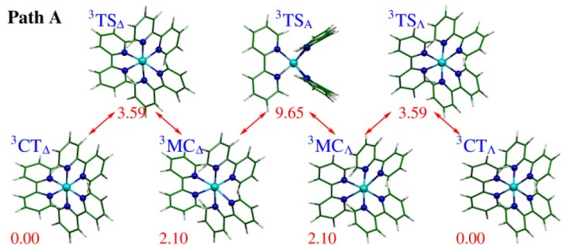

(a) Chiral inversion path of $[Ru(bipy)_3]^{2+}$

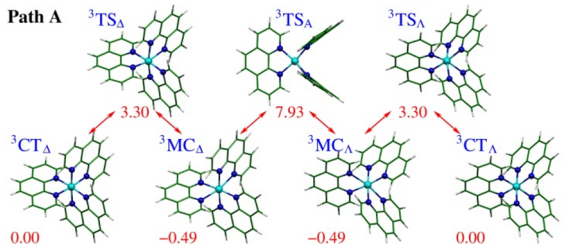

(b) Chiral inversion path of $[Ru(phen)_3]^{2+}$

Figure 4. Optimized structures of the triplet excited states involved in the rhombic inversion pathways of $[Ru(bipy)_3]^{2+}$ (a) and $[Ru(phen)_3]^{2+}$ (b), respectively. The energies are in kilocalories per mole.

though they are chemically very stable. As far as the photoinduced chiral inversion $\Delta \rightleftharpoons \Lambda$ is considered, it consists of three steps: $^3CT_\Delta \rightleftharpoons {}^3MC_\Delta$, $^3MC_\Delta \rightleftharpoons {}^3MC_\Lambda$, and $^3MC_\Lambda \rightleftharpoons {}^3CT_\Lambda$. From Figure 4 we see that the second step $^3MC_\Delta \rightleftharpoons {}^3MC_\Lambda$ is the rate-determining step (RDS) for both the bipy and phen complexes, because it has the highest energy barrier of ~7.55 kcal/mol (bipy) or 8.42 kcal/mol (phen), while those of the first and the third steps are less than 3.79 kcal/mol. This is quite different from that of the $[Ru(diimine)_2(L\text{-}ser)]^+$ complexes.[22] In the latter case, the first forward and the third backward steps are the RDS, while the second is a fast process of nanoseconds, which guarantees their chiral inversion $\Delta(\delta S) \rightleftharpoons \Lambda(\delta S)$ to be reversible with no ligand release or substitutions. However, for the prototype complexes $[Ru(bipy)_3]^{2+}$ and $[Ru(phen)_3]^{2+}$, the key step $^3MC_\Delta \rightleftharpoons {}^3MC_\Lambda$ is just an RDS, which leads to the excited Δ/Λ isomers accumulating on the ^{3}MC states until the first step $^3CT_\Delta \rightleftharpoons {}^3MC_\Delta$ approaches the thermodynamic equilibrium in given radiation field. Therefore, it is responsible for their fast decay, ligand release, and/or substitutions. To see this clearly, it is necessary to quantitatively estimate the time scales or rate constants of the processes. According to the Eyring's transition-state theory[36] (TST), the rate constant[37] $k^{TST} = \kappa(k_B T/h)\exp(-\Delta G^{\ddagger}/RT)$ of a process could be calculated from the difference $\Delta G^{\ddagger}$ in Gibbs free energy of the transition

Table 4. Main Bond Lengths (Å) and Bond and Dihedral[a] Angles (in deg) for the ^{3}CT, ^{3}MC, and ^{3}TS Triplet States of the $[Ru(bipy)_3]^{2+}$ and $[Ru(phen)_3]^{2+}$ Chelates

	$[Ru(bipy)_3]^{2+}$ (T_1)				$[Ru(phen)_3]^{2+}$ (T_1)			
triplet states	$^3CT_\Delta$	$^3TS_\Delta$	$^3MC_\Delta$	$^3TS_\Lambda$	$^3CT_\Delta$	$^3TS_\Delta$	$^3MC_\Delta$	$^3TS_\Lambda$
$Ru-N_1$	2.089	2.088	2.094	2.172	2.116	2.097	2.110	2.171
$Ru-N_5$	2.058	2.109	2.153	2.172	2.097	2.262	2.150	2.171
$Ru-N_2$	2.113	2.096	2.096	2.528	2.089	2.104	2.110	2.559
$Ru-N_6$	2.058	2.197	2.468	2.526	2.121	2.268	2.497	2.559
$Ru-N_3$	2.113	2.251	2.453	2.095	2.055	2.102	2.497	2.107
$Ru-N_4$	2.089	2.156	2.156	2.096	2.068	2.089	2.151	2.107
mean	2.087	2.150	2.237	2.265	2.091	2.154	2.252	2.279
N_1-Ru-N_2	77.74	77.68	77.55	68.22	79.01	79.09	78.33	69.16
N_5-Ru-N_6	79.68	76.70	71.56	68.23	78.74	73.14	71.90	69.16
N_3-Ru-N_4	77.74	74.41	71.37	77.31	80.73	79.54	71.89	78.17
N_1-Ru-N_3	99.09	101.98	105.18	97.89	96.26	97.04	104.91	96.91
N_4-Ru-N_5	86.15	85.20	85.62	97.96	86.73	86.89	86.76	96.91
N_5-Ru-N_1	97.11	98.85	98.43	82.96	98.43	97.18	97.51	83.97
mean	86.25	85.81	84.95	82.09	86.65	85.48	85.22	82.38
$D(L_1L_2)$	83.51	77.55	76.90	84.00	85.75	86.28	80.25	81.02
$D(L_1L_3)$	83.21	73.83	74.44	−63.46	85.00	88.70	80.27	70.60
$D(L_2L_3)$	83.21	83.50	85.51	−83.56	83.88	89.98	87.33	−81.02

[a] $D(L_1L_2)$ is the dihedral angle between the ligands L_1 and L_2 (cf. Figure 2), which is determined by their planes of inertia.

DOI: 10.1021/acs.inorgchem.8b00975
Inorg. Chem. XXXX, XXX, XXX−XXX

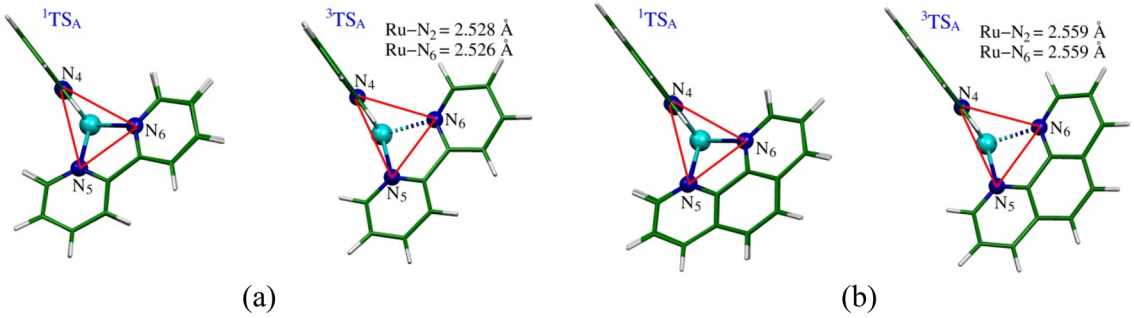

Figure 5. Comparison of the rhombic transition-state geometries between singlet S_0 and triplet T_1 state for the $[Ru(bipy)_3]^{2+}$ (a) and $[Ru(phen)_3]^{2+}$ (b) complexes.

state and the reactant, where the transmission coefficient κ could be estimated with the Wigner tunnelling correction[38] $\kappa = 1 + (1/24)[h\mathrm{Im}(\nu^{\ddagger})/k_BT]^2$. The correction involves only the transition-state imaginary-frequency $\mathrm{Im}(\nu^{\ddagger})$. All other symbols have their normal meanings. In this way, the rate constants k_q and k_{-q} for the forward and backward three steps (q = 1, 2, 3) were calculated, and the corresponding time scales defined by the reciprocal of rate constants $\tau_q = 1/k_q$, $\tau_{-q} = 1/k_{-q}$, are as follows:

$$\tau_1 = \tau_{-3} = 14.1 \text{ ps}, \ \tau_{-1} = \tau_3 = 7.89 \text{ ps},$$
$$\tau_2 = \tau_{-2} = 0.437 \ \mu\text{s}, \text{ for } [Ru(bipy)_3]^{2+}$$

$$\tau_1 = \tau_{-3} = 17.9 \text{ ps}, \ \tau_{-1} = \tau_3 = 1.23 \text{ ps},$$
$$\tau_2 = \tau_{-2} = 7.05 \ \mu\text{s}, \text{ for } [Ru(phen)_3]^{2+}$$

It is evident that the key step $^3MC_\Delta \rightleftharpoons {}^3MC_\Lambda$ is a very slow process of microseconds, while the CT-to-MC steps are fast ones of picoseconds. The latter is in good agreement with the observed value[39] of ∼50 ps for $[Ru(bipy)_3]^{2+}$ and a few picoseconds for its derivatives,[40] though the former has not been reported in literature yet. To judge the possibility of the key step in time-scale, we need the radiative lifetime of $[Ru(bipy)_3]^{2+}$ in aqueous solution. It is ∼15 μs as reported by van Houten and Watts.[41] Later it was reevaluated by Suzuki et al.[42] as 9.2 μs. Therefore, the racemization of the bipy and phen complexes could take place, but generally it may not have sufficient time to complete. This accounts for the fact that their photochemical reactions are dominated by the photolysis or photosubstitutions, not by the photoracemization.

Optimized Geometries of the ^{3}TS and Related States. The transition-state structures are one of the important factors to understand the photochemical processes and photodissociation products. Table 4 compiles the selected bond lengths, bond angles, and dihedral angles for the ^{3}CT, ^{3}MC, and ^{3}TS triplet states of the Δ enantiomer in the rhombic inversion. The Λ-enantiomer has the same bond parameters as the Δ-isomer except for the dihedral angles, which are the same in magnitude but opposite in sign. Moreover, in the Ray-Dutt twist (Figure 3a), the mirror-image relationships of nitrogen atoms between the Δ and Λ enantiomers are $N_1 \sim N_5$, $N_2 \sim N_6$, and $N_3 \sim N_4$; for example, the mirror image of N_1 in Δ isomer is N_5 in Λ isomer. Thus, in the first step $^3CT_\Delta \rightarrow {}^3MC_\Delta$, the octahedral core $\{RuN_6\}$ of the Δ isomer is elongated by ∼18% (bipy) or 20% (phen) along the N_3−Ru−N_6 axis. Meanwhile, the N_5−Ru−N_6 and N_3−Ru−N_4 bite angles decrease gradually by ∼10%. The second step $^3MC_\Delta \rightarrow {}^3MC_\Lambda$ is identified by the Ray-Dutt twist (Figure 3a), which makes the distance of Ru−N_3 decrease rapidly to 2.095 Å (bipy) or 2.107 Å (phen) at the key transition state ^3TS_A and makes that of Ru−N_2 increase rapidly to 2.528 Å (bipy) or 2.559 Å (phen). This directly leads to the Ru atom shift to one of the side face composed of N_1, N_3, N_4, and N_5, as depicted in Figure 5. Just in this step, the long axis of the octahedral core changes from the N_3−Ru−N_6 of $^3MC_\Delta$ to N_4−Ru−N_2 of $^3MC_\Lambda$ via the achiral ^3TS_A structure. The third step $^3MC_\Lambda \rightarrow {}^3CT_\Lambda$ is a recover procedure of the octahedral core, where Ru−N_4 and Ru−N_2 bond lengths decrease gradually to the normal values. Also the two bond lengths Ru−N_1 and Ru−N_5 change slightly during all the three steps. To see the geometrical change clearly, two videos for the chiral inversion were prepared and presented in the Supporting Information. Additionally, Figure 5 indicates that the structures of ^1TS_A are regular rhombic forms with the body-centered Ru in the ground state S_0. However, in the triplet excited state T_1, such forms are significantly distorted with two much-weakened Ru−N bonds due to the shift of Ru atom to the side face. In which, the Ru(II) atom and the nearest four nitrogens form a flatten square pyramid (FSP) structure with a height of 0.276 and 0.283 Å for the bipy and phen complexes, respectively. Therefore, strictly speaking, the chiral inversion patterns in T_1 state are not a typical rhombic twist, but mixed with bond rupture forms, at least partly.

The Mechanism of Photoracemization. To understand the mechanisms of photolysis and photoracemization of the complexes, the relaxed energy curve of the triplet T_1 state along the $^3MC_\Delta \rightleftharpoons {}^3MC_\Lambda$ inversion path, together with those of the singlet S_0 and other lower-energy excited states (T_2, T_3, and S_1) calculated at the optimized structures of T_1, are depicted in Figure 6. Whereas the structures of $^3MC_\Delta$, ^3TS_A, and $^3MC_\Lambda$ are fully optimized, the pathways from $^3MC_\Delta$ to ^3TS_A and from ^3TS_A to $^3MC_\Lambda$ are characterized by the geometry interpolation ratio p and $1 + p'$ ($0 \le p, p' \le 1$), respectively. The interpolation geometries were optimized with restriction of fixed relative orientations of ligands L_1, L_2, and L_3. The color dots and lines denote the calculated energies and fitting curves, respectively. Clearly, in the chiral inversion $^3MC_\Delta \rightleftharpoons {}^3MC_\Lambda$, the triplet excited state T_1 becomes ground state at both sides of ^3TS_A due to the intersection of T_1 and S_0. The other lower-energy excited states, including the second and the third triplet states (T_2 and T_3), as well as the first singlet excited state S_1, have no perceptible influence on this intersection. In addition, Figure 6 indicates that the two crossing points appear at approximately three tenths and seven tenths of the inversion path. Their energies are 0.245 eV (5.65 kcal/mol) above the bottom of corresponding ^{3}MC state.

DOI: 10.1021/acs.inorgchem.8b00975
Inorg. Chem. XXXX, XXX, XXX−XXX

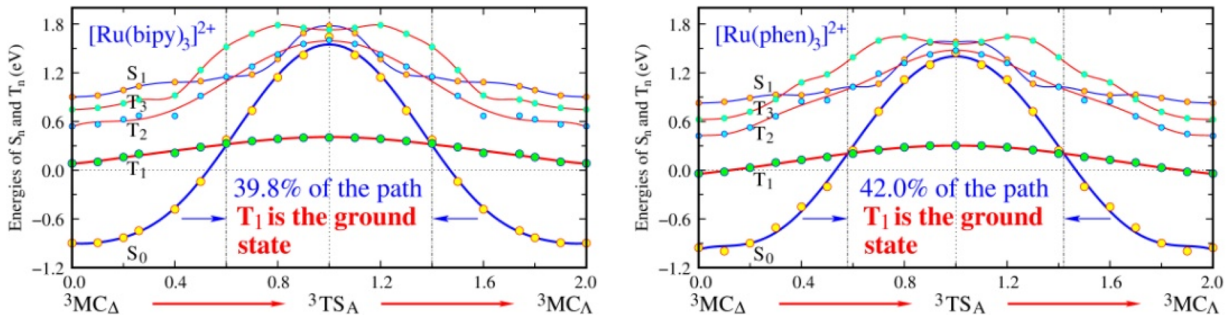

Figure 6. Potential energy curves of the relaxed T_1 and vertical S_0, S_1, T_2, and T_3 states of the $[Ru(bipy)_3]^{2+}$ (left) and $[Ru(phen)_3]^{2+}$ (right) complexes along the rhombic inversion pathway of $^3MC_\Delta \rightleftharpoons {}^3MC_\Lambda$.

Examining the transient geometries at the crossing points, we found that the imaginary-frequency displacement vectors in the T_1 state are parallel to the reaction path and deviate from the path in the S_0 state. The latter is a stretch mode and thus may lead to ligand dissociation by coupling with corresponding vibration. All these features are similar to the photoinduced chiral inversion of the $[Ru(bipy)_2(L\text{-}ser)]^+$ series complexes.[22] So it is also a triplet ground-state bridged photochemical process, where the ground-state character of ^3TS_A guarantees the chiral inversion proceeding. However, different from the $[Ru(bipy)_2(L\text{-}ser)]^+$ systems, the inversion process $^3MC_\Delta \rightleftharpoons {}^3MC_\Lambda$ for the prototype complexes $[Ru(bipy)_3]^{2+}$ and $[Ru(phen)_3]^{2+}$ is the RDS with a time scale of microseconds. In this case the excited system will linger around or accumulate at the bottom of ^3MC state, until the first step approaches the thermal equilibrium, which may greatly enhance the possibility of deexcitation via nonradiative transitions or ligand dissociations. Heully et al.[43] thought that an efficient decay occurs through a deactivation funnel that is the crossing point between the ^3MC and the ground state S_0 potential energy surfaces. Checking the geometries at the crossing points, it is found that the two bonds $Ru-N_2$ and $Ru-N_6$ are much weakened with lengths of 2.493 and 2.401 Å for $[Ru(bipy)_3]^{2+}$ or 2.504 and 2.426 Å for $[Ru(phen)_3]^{2+}$. As a result, the ligands **1** and **3** become almost monocoordinated and behave more freely. They can readily decay to the ground-state surface S_0 due to molecular vibrations. The ground state in such a distorted geometry can return to its equilibrium geometry, but it may also interact with solvent molecules,[44] yielding a photosubstitution or photolysis product. Direct optimization of the ^3MC structures at the left and right crossing points with singlet constraint yields the ground-state structures Δ and Λ, respectively. This indicates that the opposite enantiomer of a reactant found in the photoproducts was formed before it decays to the singlet ground state, not after. Therefore, there are two pathways for the racemization of the complexes: (1) the reactant goes through the three steps $^3CT_\Delta \rightleftharpoons {}^3MC_\Delta$, $^3MC_\Delta \rightleftharpoons {}^3MC_\Lambda$, and $^3MC_\Lambda \rightleftharpoons {}^3CT_\Lambda$, then returns to the ground state S_0 by photon emitting; (2) the reactant goes through the first two steps then decays to the ground state at the crossing point near the product. The latter might be negligible, because the third step is a fast process of picoseconds. So the former is the dominant pathway of the racemization and is reversible in the sense of energy conservation. Nevertheless, both pathways involve the key step $^3MC_\Delta \rightleftharpoons {}^3MC_\Lambda$; that is, the chiral inversion or racemization is actually performed on the triplet ground state around ^3TS_A, not on the singlet (S_0) one.

According to above discussions, the photolysis involved processes were also depicted in Figure 1 by the dashed lines at both sides of ^3TS. In this case, the second step of the forward reaction Δ → Λ is dominated by $^3MC_\Delta \rightarrow S_0(\Delta)$ mostly at the crossing point, while the possibility of $^3MC_\Lambda \rightarrow S_0(\Lambda)$ is neglectable, as the third step $^3MC_\Lambda \rightarrow {}^3CT_\Lambda$ is a fast one. Similarly, the second step of the backward reaction Δ ← Λ would be dominated by $^3MC_\Lambda \rightarrow S_0(\Lambda)$, and the possibility of $^3MC_\Delta \rightarrow S_0(\Delta)$ could be neglected.

Concerning the mechanism suggested in ref 12, it involves the bond-rupture model[28] (Figure 7) and requires rearrangement of the square pyramidal primary photoproduct (Figure 7b) into a five-coordinate intermediate with the trigonal bipyramid geometry (Figure 7c). This model is deceptively simple yet wildly hard to handle. Our preliminary investigations showed that the trigonal bipyramid transition state is difficult to locate due to the influence of the monocoordinate ligand. Moreover, with simulations on the photolysis product by taking geometries on the inversion path $^3MC_\Delta \rightleftharpoons {}^3MC_\Lambda$, modified with different displacement vectors of their normal models, no clue was found for racemizations on the potential energy surface S_0. Of course, we could not preclude the bond-rupture mechanism based on these facts, but the possibility would be small, since it is also not consistent with other experiments.

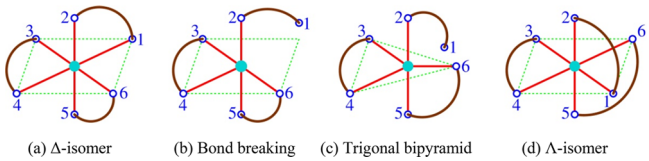

Figure 7. Bond-rupture model for the Δ → Λ racemization of a six-coordinate complex.

However, according to the mechanism suggested in this Paper, the racemization of the complexes is irrelevant to the photoproduct. It is the RDS that controls the competition between photolysis and photoracemization. For the $[Ru(bipy)_2(L\text{-}ser)]^+$ series complexes, the chiral inversion is reversible with no detectable photolysis, as it is a fast process, while for the $[Ru(bipy)_3]^{2+}$ series complexes, the photolysis is the main photochemical reaction, because the racemization as the RDS is suffocated. In this case, the chiral inversion of the prototype complexes still passes through three steps and ends with a photon emitting, which could be detected using the circularly polarized luminescence (CPL)[45] and related techniques[46,47] experimentally.

DOI: 10.1021/acs.inorgchem.8b00975
Inorg. Chem. XXXX, XXX, XXX−XXX

CONCLUSIONS

A detailed analysis on the photoracemization of the $[Ru(bipy)_3]^{2+}$ and $[Ru(phen)_3]^{2+}$ prototype complexes is presented at the first-principle level of theory. The results indicate that the photoracemization reaction $\Delta \rightleftharpoons \Lambda$ of the complexes takes place on the lowest triplet excited state T_1 potential energy surface in three steps: $^3CT_\Delta \rightleftharpoons {}^3MC_\Delta$, $^3MC_\Delta \rightleftharpoons {}^3MC_\Lambda$, and $^3MC_\Lambda \rightleftharpoons {}^3CT_\Lambda$, where the first and third steps mainly involve the elongation and compression of the octahedral core of the Δ and Λ enantiomers, respectively. The $\Delta \leftrightarrow \Lambda$ chiral inversion occurs in the second step via a much-distorted square-pyramid-like transition-state structure ^3TS_A. All these features are same as the photoinduced chiral inversion of the $[Ru(bipy)_2(L\text{-}ser)]^+$ series complexes.[22] So it is also a triplet ground-state bridged photochemical process.

However, different from the $[Ru(bipy)_2(L\text{-}ser)]^+$ systems, the key inversion process $^3MC_\Delta \rightleftharpoons {}^3MC_\Lambda$ for the prototype complexes is the RDS with a time scale of microseconds. In this case the excited system will linger around the bottom of ^3MC state after the first step and, therefore, greatly enhance the possibility of deexcitation via nonradiative transitions or ligand dissociations. In other words, RDS is the key factor dominating the competition between photolysis and photoracemization in these and related complexes. This conclusion is helpful in understanding and controlling the photochemical behavior of the complexes in practice.

ASSOCIATED CONTENT

Supporting Information

The Supporting Information is available free of charge on the ACS Publications website at DOI: 10.1021/acs.inorgchem.8b00975.

Complete ref 34; the optimized Cartesian coordinates for all the metastable and transition-state geometries involved in the photoracemization of $[Ru(bipy)_3]^{2+}$ and $[Ru(phen)_3]^{2+}$ (PDF)

Video showing the rhombic inversion of $[Ru(bipy)_3]^{2+}$ (AVI)

Video showing the rhombic inversion of $[Ru(phen)_3]^{2+}$ (AVI)

AUTHOR INFORMATION

Corresponding Author

*E-mail: ykwang@sxu.edu.cn.

ORCID

Yuekui Wang: 0000-0001-8435-1980

Notes

The authors declare no competing financial interest.

ACKNOWLEDGMENTS

We gratefully acknowledge the financial support from the National Natural Science Foundation of China (Grant No. 21273139).

REFERENCES

(1) Campagna, S.; Puntoriero, F.; Nastasi, F.; Bergamini, G.; Balzani, V. Photochemistry and Photophysics of Coordination Compounds: Ruthenium. *Top. Curr. Chem.* **2007**, *280*, 117−214.

(2) Kalyanasundaram, K. Photophysics, Photochemistry and Solar Energy Conversion with Tris(bipyridyl)ruthenium(II) and its Analogues. *Coord. Chem. Rev.* **1982**, *46*, 159−244.

(3) Juris, A.; Balzani, V.; Barigelletti, F.; Campagna, S.; Belser, P.; Von Zelewsky, A. Ru(II) Polypyridine Complexes: Photophysics, Photochemistry, Electrochemistry, and Chemiluminescence. *Coord. Chem. Rev.* **1988**, *84*, 85−277.

(4) Demas, J. N.; Crosby, G. A. Quantum Efficiencies on Transition Metal Complexes. II. Charge-Transfer Luminescence. *J. Am. Chem. Soc.* **1971**, *93*, 2841−2847.

(5) Crosby, G. A. Spectroscopic Investigations of Excited States of Transition- Metal Complexes. *Acc. Chem. Res.* **1975**, *8*, 231−238.

(6) Puntoriero, F.; Sartorel, A.; Orlandi, M.; La Ganga, G.; Serroni, S.; Bonchio, M.; Scandola, F.; Campagna, S. Photoinduced Water Oxidation Using Dendrimeric Ru(II) Complexes as Photosensitizers. *Coord. Chem. Rev.* **2011**, *255*, 2594−2601.

(7) Zhao, Y.; Swierk, J. R.; Megiatto, J. D., Jr; Sherman, B.; Youngblood, W. J.; Qin, D.; Lentz, D. M.; Moore, A. L.; Moore, T. A.; Gust, D.; Mallouk, T. E. Improving the Efficiency of Water Splitting in Dye-sensitized Solar Cells by Using a Biomimetic Electron Transfer Mediator. *Proc. Natl. Acad. Sci. U. S. A.* **2012**, *109*, 15612−15616.

(8) Demas, J. N.; DeGraff, B. A. Design and Applications of Highly Luminescent Transition Metal Complexes. *Anal. Chem.* **1991**, *63*, 829A−837A.

(9) *Applied Photochemistry;* Evans, R. C., Douglas, P., Burrows, H. D., Eds.; Springer: Netherlands, 2013.

(10) Knoll, J. D.; Turro, C. Control and Utilization of Ruthenium and Rhodium Metal Complex Excited States for Photoactivated Cancer Therapy. *Coord. Chem. Rev.* **2015**, *282*−*283*, 110−126.

(11) Howerton, B. S.; Heidary, D. K.; Glazer, E. C. Strained Ruthenium Complexes Are Potent Light-Activated Anticancer Agents. *J. Am. Chem. Soc.* **2012**, *134*, 8324−8327.

(12) Durham, B.; Caspar, J. V.; Nagle, J. K.; Meyer, T. J. Photochemistry of $Ru(bpy)_3^{2+}$. *J. Am. Chem. Soc.* **1982**, *104*, 4803−4810.

(13) Watts, R. J.; Harrington, J. S.; Van Houten, J. Photochemical and Photophysical Processes in 2,2′-Bipyridine Complexes of Iridium(III) and Ruthenium(II). *Adv. Chem. Ser.* **1978**, *168*, 57−72.

(14) Ford, P. C. The Ligand Field Photosubstitution Reactions of d^6 Hexacoordinate Metal Complexes. *Coord. Chem. Rev.* **1982**, *44*, 61−82.

(15) Van Houten, J.; Watts, R. J. Photochemistry of Tris(2,2′-bipyridyl)-ruthenium(II) in Aqueous Solutions. *Inorg. Chem.* **1978**, *17*, 3381−3385.

(16) Porter, G. B.; Sparks, R. H. Photoracemization of Ru(Bipyridine)$_3^{2+}$. *J. Photochem.* **1980**, *13*, 123−131.

(17) Brandt, W. W.; Smith, G. F. Polysubstituted 1,10-Phenanthrolines and Bipyridines as Multiple Range Redox Indicators. *Anal. Chem.* **1949**, *21*, 1313−1319.

(18) Burstall, F. H. 34. Optical Activity Dependent on Coordinated Bivalent Ruthenium. *J. Chem. Soc.* **1936**, 173−175.

(19) Drahoňovský, D.; Knof, U.; Jungo, L.; Belser, T.; Neels, A.; Labat, G. C.; Stoeckli-Evans, H.; Von Zelewsky, A. Stereoselectivity in the Formation of Tris-diimine Complexes of Fe(II), Ru(II), and Os(II) with a C_2-symmetric Chiral Derivative of 2,2′-bipyridine. *Dalton Trans.* **2006**, 1444−1454.

(20) Vagg, R. S.; Williams, P. A. Chiral Metal Complexes. 1. Photochemical Inversion in Ternary Ru(II) Complexes of Diimines and L-Tryptophane. *Inorg. Chim. Acta* **1981**, *51*, 61−65.

(21) Vagg, R. S.; Williams, P. A. Chiral Metal Complexes. 2. Light-Catalysed Diastereoisomeric Equilibration in Aqueous Solutions of *cis*-$[Ru(phen)_2(L\text{-}Serine)]^+$ and Its 2,2′-Bipyridyl Analogue. *Inorg. Chim. Acta* **1981**, *52*, 69−72.

(22) Feng, L.; Wang, Y.; Jia, J. Triplet Ground-State-Bridged Photochemical Process: Understanding the Photoinduced Chiral Inversion at the Metal Center of $[Ru(phen)_2(L\text{-}ser)]^+$ and Its Bipy Analogues. *Inorg. Chem.* **2017**, *56*, 14467−14476.

(23) Henry, W.; Coates, C. G.; Brady, C.; Ronayne, K. L.; Matousek, P.; Towrie, M.; Botchway, S. W.; Parker, A. W.; Vos, J. G.; Browne, W. R.; McGarvey, J. J. The Early Picosecond Photophysics of Ru(II) Polypyridyl Complexes: A Tale of Two Timescales. *J. Phys. Chem. A* **2008**, *112*, 4537−4544.

DOI: 10.1021/acs.inorgchem.8b00975
Inorg. Chem. XXXX, XXX, XXX−XXX

(24) Wagenknecht, P. S.; Ford, P. C. Metal Centered Ligand Field Excited States: Their Roles in the Design and Performance of Transition Metal Based Photochemical Molecular Devices. *Coord. Chem. Rev.* **2011**, *255*, 591−616.
(25) Sun, Q.; Mosquera-Vazquez, S.; Suffren, Y.; Hankache, J.; Amstutz, N.; Lawson Daku, L. M.; Vauthey, E.; Hauser, A. On the Role of Ligand-Field States for the Photophysical Properties of Ruthenium(II) Polypyridyl Complexes. *Coord. Chem. Rev.* **2015**, *282*−*283*, 87−99.
(26) Bailar, J. C., Jr. Some Problems in the Stereochemistry of Coordination Compounds. *J. Inorg. Nucl. Chem.* **1958**, *8*, 165−175.
(27) Rây, P.; Dutt, N. K. Kinetics and Mechanism of Racemization of Optically Active Cobaltic Trisbiguanide Complex. *J. Indian Chem. Soc.* **1943**, *20*, 81−92.
(28) Hutchison, J. R.; Gordon, J. G.; Holm, R. H. Intramolecular Rearrangement Reactions of Tris-Chelate Complexes. II. Kinetics and Probable Mechanism of the Isomerization and Racemization of the "Fast" Complexes Tris(l-phenyl-5-methylhexane-2,4-dionato)-aluminum(III) and -gallium(III). *Inorg. Chem.* **1971**, *10*, 1004−1017.
(29) Stephens, P. J.; Devlin, F. J.; Chabalowski, C. F.; Frisch, M. J. *Ab Initio* Calculation of Vibrational Absorption and Circular Dichroism Spectra Using Density Functional Force Fields. *J. Phys. Chem.* **1994**, *98*, 11623−11627.
(30) Martin, J. M. L.; Sundermann, A. Correlation Consistent Valence Basis Sets for Use with the Stuttgart-Dresden-Bonn Relativistic Effective Core Potentials: The Atoms Ga-Kr and In-Xe. *J. Chem. Phys.* **2001**, *114*, 3408−3420.
(31) Andrae, D.; Häußermann, U.; Dolg, M.; Stoll, H.; Preuß, H. Energy-Adjusted *ab initio* Pseudopotentials for the Second and Third Row Transition Elements. *Theor. Chim. Acta* **1990**, *77*, 123−141.
(32) Fukui, K. The Path of Chemical-Reactions − The IRC Approach. *Acc. Chem. Res.* **1981**, *14*, 363−368.
(33) Ruiz, E.; Cirera, J.; Alvarez, S. Spin Density Distribution in Transition Metal Complexes. *Coord. Chem. Rev.* **2005**, *249*, 2649−2660.
(34) Frisch, M. J.; Trucks, G. W.; Schlegel, H. B.; et al. *Gaussian 09, Revision B.01;* Gaussian, Inc.: Wallingford, CT, 2010 (see Supporting Information for full reference).
(35) Tomasi, J.; Mennucci, B.; Cammi, R. Quantum Mechanical Continuum Solvation Models. *Chem. Rev.* **2005**, *105*, 2999−3093.
(36) Eyring, H. The Activated Complex in Chemical Reactions. *J. Chem. Phys.* **1935**, *3*, 107−115.
(37) Laidler, K. J.; King, M. C. The Development of Transition-State Theory. *J. Phys. Chem.* **1983**, *87*, 2657−2664.
(38) Wigner, E. Über das Überschreiten von Potentialschwellen bei chemischen Reaktionen. *Z. Phys. Chem.* **1932**, *19B*, 203−216.
(39) Mukuta, T.; Tanaka, S.; Inagaki, A.; Koshihara, S.; Onda, K. Direct Observation of the Triplet Metal-Centered State in $[Ru(bpy)_3]^{2+}$ Using Time-Resolved Infrared Spectroscopy. *Chem. Select* **2016**, *1*, 2802−2807.
(40) Sun, Q.; Mosquera-Vazquez, S.; Lawson Daku, L. M.; Guénée, L.; Goodwin, H. A.; Vauthey, E.; Hauser, A. Experimental Evidence of Ultrafast Quenching of the ^{3}MLCT Luminescence in Ruthenium(II) Tris-bipyridyl Complexes via a ^{3}dd State. *J. Am. Chem. Soc.* **2013**, *135*, 13660−13663.
(41) Van Houten, J.; Watts, R. J. Temperature Dependence of the Photophysical and Photochemical Properties of the Tris(2,2′-bipyridyl)ruthenium(II) Ion in Aqueous Solution. *J. Am. Chem. Soc.* **1976**, *98*, 4853−4858.
(42) Suzuki, K.; Kobayashi, A.; Kaneko, S.; Takehira, K.; Yoshihara, T.; Ishida, H.; Shiina, Y.; Oishi, S.; Tobita, S. Reevaluation of Absolute Luminescence Quantum Yields of Standard Solutions Using a Spectrometer with an Integrating Sphere and a Back-thinned CCD Detector. *Phys. Chem. Chem. Phys.* **2009**, *11*, 9850−9860.
(43) Heully, J.-L; Alary, F.; Boggio-Pasqua, M. Spin-orbit Effects on the Photophysical Properties of $[Ru(bpy)_3]^{2+}$. *J. Chem. Phys.* **2009**, *131*, 184308−184308−9.
(44) Thompson, D. W.; Wishart, J. F.; Brunschwig, B. S.; Sutin, N. Efficient Generation of the Ligand Field Excited State of Tris-(2,2′-bipyridine)-ruthenium(II) through Sequential Two-Photon Capture by $[Ru(bpy)_3]^{2+}$ or Electron Capture by $[Ru(bpy)_3]^{3+}$. *J. Phys. Chem. A* **2001**, *105*, 8117−8122.
(45) Longhi, G.; Castiglioni, E.; Koshoubu, J.; Mazzeo, G.; Abbate, S. Circularly Polarized Luminescence: A Review of Experimental and Theoretical Aspects. *Chirality* **2016**, *28*, 696−707.
(46) Schauerte, J. A.; Steel, D. G.; Gafni, A. Time-resolved Circularly Polarized Protein Phosphorescence. *Proc. Natl. Acad. Sci. U. S. A.* **1992**, *89*, 10154−10158.
(47) Riehl, J. P.; Muller, G. Circularly Polarized Luminescence Spectroscopy and Emission-Detected Circular Dichroism. In *Comprehensive Chiroptical Spectroscopy;* Berova, N., Polavarapu, P. L., Nakanishi, K., Woody, R. W., Eds.; Wiley & Sons: Hoboken, NJ, 2012; Vol. *1*, pp 65−90.

DOI: 10.1021/acs.inorgchem.8b00975
Inorg. Chem. XXXX, XXX, XXX−XXX